How well can modified gravitational wave propagation be constrained with strong lensing?

Harsh Narola,[1,2] Justin Janquart,[1,2] Leïla Haegel,[3] K. Haris,[1,2,4] Otto A. Hannuksela,[5] and Chris Van Den Broeck[1,2]

[1]*Institute for Gravitational and Subatomic Physics (GRASP), Utrecht University, Princetonplein 1, 3584 CC Utrecht, The Netherlands*
[2]*Nikhef—National Institute for Subatomic Physics, Science Park 105, 1098 XG Amsterdam, The Netherlands*
[3]*Université Paris Cité, CNRS, Astroparticule et Cosmologie, F-75013 Paris, France*
[4]*Department of Physics, National Institute of Technology, Kozhikode, Kerala 673601, India*
[5]*Department of Physics, The Chinese University of Hong Kong, Shatin, New Territories, Hong Kong*

(Received 7 August 2023; accepted 29 March 2024; published 25 April 2024)

Strong gravitational lensing produces multiple images of a gravitational wave (GW) signal, which can be observed by detectors as time-separated copies of the same event. It has been shown that under favorable circumstances, by combining information from a quadruply lensed GW with electromagnetic observations of lensed galaxies, it is possible to identify the host galaxy of a binary black hole coalescence. Comparing the luminosity distance obtained through electromagnetic means with the effective luminosity distance inferred from the lensed GW signal would then enable us to constrain alternative theories of gravity that allow for modified GW propagation. Here we analyze models including large extra spatial dimensions, a running Planck mass, and a model that captures propagation effects occurring in a variety of alternative theories to general relativity. We consider a plausible population of lenses and binary black holes and use Bayesian inference on simulated GW signals as seen in current detectors at design sensitivity, to arrive at a realistic assessment of the bounds that could be placed. We find that, due to the fact that the sources of lensed events will typically be at much larger redshifts, this method can improve over bounds from GW170817 and its electromagnetic counterpart by a factor of ~ 5 to $\mathcal{O}(10^2)$, depending on the alternative gravity model.

DOI: 10.1103/PhysRevD.109.084064

I. INTRODUCTION

Since the first direct detection of gravitational waves (GWs) in 2015, the field of GW physics has been developing rapidly [1]. The network of two Advanced LIGO detectors [2] and one Advanced Virgo detector [3] has observed around 90 GW signals to date [4]. These observations have opened up several previously unexplored research directions. For example, they have led to enhanced tests of general relativity (GR) by providing access to the genuinely strong-field dynamics of spacetime [5], provided a new method for probing the expansion of the Universe [6], and contributed to a better understanding of the formation channels of the binaries and other astrophysical compact objects [7]. As the interferometers' sensitivities improve and new detectors such as KAGRA [8–11] and LIGO-India [12] join the network, even more events will be observed.

The detector upgrades could enable the detection of new phenomena, such as the gravitational lensing of GWs [13–15]. The latter occurs when GWs experience deflection due to a massive object, known as the lens, in their path. Recent rate estimates suggest that GW lensing can become detectable at the rate of $\mathcal{O}(1)$ per year with current detectors at design sensitivity [16–22]. If the Schwarzschild radius of the lens is much larger than the GW wavelength (i.e. when the geometric optics limit applies), it can split the observed GW signal into multiple copies, also referred to as the lensed images. Typically we expect to see up to four images; a fifth image will generally be strongly demagnified and difficult to detect [23]. This phenomenon is called the strong lensing of gravitational waves. The images reach the detector as repeated and time-separated copies of the GW signals that only differ in their amplitudes (due to being magnified/demagnified by the lens), overall phases (due to image inversion along one or two principal axes), and arrival times (as the images travel along trajectories of different length) [24,25]. By contrast, if the size of the lens is comparable to the wavelength of the GW (referred to as the wave optics limit), the GW can undergo frequency-dependent modulation [26–36].

Gravitational lensing has several interesting applications in fundamental physics, cosmology, and astrophysics (for example see Refs. [37–59]). Our work focuses on strong lensing and its ability to test GW propagation beyond GR. In particular, it enables tests of theories and models with modified GW propagation. Here we will focus on three different (classes of) models: one which has large extra spatial dimensions [60]; one where anomalous propagation arises from a time-varying Planck mass [61]; and another one proposed in [62] which captures propagation effects in a number of alternative theories of gravity [63], and which here we will refer to as Ξ parametrization. Recent studies have already demonstrated that the latter can be tested using strongly lensed events [64]. Here we provide a comprehensive assessment of the constraints that can be placed on all of the above mentioned models, assuming realistic distributions for the parameters characterizing the lenses and the binary black holes, for second-generation GW detectors at design sensitivity.

A strongly lensed GW source will have an improved sky localization compared to a nonlensed source, as we can observe the former multiple times with different detector orientations [65–69]. Especially with four detectable images,[1] we may be able to localize the source within $\mathcal{O}(1)$ square degrees [54,55]. When the GW source is lensed, we can expect that the electromagnetic (EM) radiation coming from its host galaxy is also lensed, as is widely assumed in cosmography studies [70–74]. A joint GW + EM analysis can help locate the source's host galaxy once its location is narrowed down to a few square degrees using only GW data. In this step, one reconstructs all the lenses in the region provided by the GW data to find which lens could best produce a GW quadruplet with properties similar to the ones observed; the galaxy that is undergoing lensing by this particular lens is then likely to be the host galaxy of the GW event. This method was proposed and studied in [54,55]. Once the host galaxy is known, a dedicated spectroscopic or photometric follow-up can lead us to the redshift of the source. By combining the source's redshift with a cosmological model, we can estimate the source's luminosity distance in a way that is unaffected by the anomalous GW propagation [75]. In addition, we can have another, independent measurement of the source's luminosity distance from the GW data, which could be affected by anomalous propagation; by comparing the two distances the anomaly can be discovered or bounded.

Let us denote by D_L^{EM} the luminosity distance derived from the EM redshift measurements and a cosmological model, which we will refer to as the EM luminosity distance. Similarly, let us write D_L^{GW} for the luminosity distance measured from the GW data when assuming an amplitude falloff proportional to $1/D_L^{\mathrm{GW}}$, and call it the GW luminosity distance. In GR, D_L^{GW} and D_L^{EM} coincide, but in alternative theories of gravity there can be a nontrivial relationship between the two. This relationship will be sensitive both to parameters associated with the deviation from GR, and to the cosmological parameters. For definiteness, in this work we will generally consider a spatially flat Friedmann-Lemaitre-Robertson-Walker (FLRW) Universe with cosmological constant and negligible radiation density, in which case the cosmological parameters are the Hubble constant H_0, and the densities of matter and dark energy relative to the critical density, respectively denoted by Ω_m and Ω_Λ. For the purposes of this study, we will fix Ω_m and Ω_Λ to their values from Planck 2018 [76], whereas H_0 will be left free. Note that in the relationship between D_L^{GW} and D_L^{EM} there will be a degeneracy between the deviation parameters and H_0 [61]. Thus, bounds on the deviation parameters will be determined by the prior information we have from previous measurements on H_0, together with the measurement uncertainty on D_L^{GW}. For H_0, we could in principle choose a fairly narrow prior range informed by the Planck [77], SHoES [78], or other previous measurements [79]. However, in our setting, information about H_0 can be obtained from the difference in times of arrival of the GW images, together with lens reconstruction through electromagnetic means, as explained in detail in [55,80]. Since the latter will typically lead to wider ranges for H_0 compared to the previous H_0 measurements, our predictions for the bounds one can obtain on the deviation parameters will be on the conservative side.

Studying modified propagation theories in the context of strongly lensed and localized GW events, especially from binary black hole (BBH) coalescences, is attractive, because such events can be detected at a higher redshift compared to binary neutron star (BNS) events. In the past, modified propagation theories have been tested using GW170817 [61,81–83], a signal from a BNS inspiral with an identifiable EM counterpart [84,85]. However, by cosmological standards, the GW170817 signal traveled only a small distance before it reached the detectors, and in modified propagation theories, the imprint of the deviation tends to accumulate with distance. Other methods have been proposed that exploit the population properties of BBH coalescences observed with GWs [86–88]; since BBHs can be detected out to larger distances, this enables considerably improved bounds over the ones from GW170817. Due to magnification, GWs from *lensed* BBH events can potentially be seen out to redshifts $z \sim 6$ [16], so that more stringent constraints can be expected also from this methodology. The aim of this paper is to quantify the gain from GW lensing for the different anomalous propagation scenarios considered.

The rest of the paper is structured as follows. In Sec. II, we recall the basics of GW lensing. Modified propagation theories are discussed in Sec. III, and our method for constraining anomalous propagation through lensing is described in Sec. IV. Results and comparisons with measurements on GW170817 and other techniques are presented in Sec. V. Finally, Sec. VI provides conclusions and future directions. We work in the geometric unit system so that the speed of light and the gravitational constant are set to unity.

[1]30% of strongly lensed events are predicted to be quadruplets [22].

II. GRAVITATIONAL-WAVE LENSING AND DISTANCE MEASUREMENTS

To understand how strongly lensed GWs can be applied to test theories with modified GW propagation, here we briefly summarize the important elements of strong lensing (for a detailed overview of GW lensing, see Ref. [13], and to understand the localization aspects, see Refs. [54,55]). We will assume that the GW is originating from a BBH coalescence and that it is strongly lensed by a galaxy, one of the most common configurations according to forecasts [16,21]. In such a scenario, the geometric optics limit applies, and multiple images of the GWs are produced.

Strong lensing introduces a magnification μ_i, a time delay t_i^d, and an overall complex phase shift πn_i, called the Morse phase, to each image. They modify the waveform as

$$h_L^i(f;\vec{\theta},\mu_i,t_i^d,n_i) = |\mu_i|^{1/2} e^{i2\pi f t_i^d - i\pi n_i} h(f;\vec{\theta}), \qquad (1)$$

where h_L^i is the waveform associated with the i^{th} lensed image, $h(f;\vec{\theta})$ is the waveform in the absence of lensing, f is the frequency, and $\vec{\theta}$ are the source parameters of the binary. The magnifications, time delays, and Morse phases can be calculated by solving the lens equation if we have information about the source position and lens properties.

Note that Eq. (1) implies that strong lensing does not change the evolution of frequency as a function of time. Since this frequency evolution is set by the masses and spins of binary black holes, the way one searches for lensed GWs is to compare measurements of these parameters in subsets of all the detected events, requiring them to be consistent for lensing to have occurred. In addition, there should be consistency between the measured sky positions. For technical details on the ways in which such searches are performed and how statistical significance is established, see Refs. [65–67,89–91].

If there is no complementary EM information available, it is not possible to disentangle the luminosity distance and magnifications just using GW data, as both only appear in the amplitudes of the images, and different images have different magnifications that are *a priori* unknown. For a given image we usually absorb the magnification into an *effective* GW luminosity distance $D_L^{\mathrm{eff,i}} = D_L^{\mathrm{GW}}/\sqrt{|\mu_i|}$. However, when EM information is at hand the magnifications can, in principle, be separately measured through lens reconstruction [92], at least for quadruply lensed events.

Suppose we have detected multiple images of a strongly lensed GW with a network of detectors. In this scenario, due to Earth's rotation in between the arrival of the different images, the same event is observed multiple times with different detector network orientations, allowing for high-accuracy sky localization [65,67]. Since at least a portion of the host galaxy of the BBH coalescence must itself be lensed, one can then consider the strongly lensed galaxies in the sky error box obtained from the GW measurements [55]. For each of these one can use the lensed EM image fluxes to reconstruct the profile of the lens. By requiring consistency with the GW relative time delays, relative magnifications, and Morse phases, one can filter out incorrect lenses and in principle pinpoint the correct lens and host galaxy. From spectroscopic or photometric measurements, the redshift of the host galaxy can be obtained. Moreover, for quadruply lensed events, the relative time delays of the GW images together with the EM reconstruction of the now identified lens enable measurement of the *absolute* magnifications μ_i [55]. Combined with GW measurements of $D_L^{\mathrm{eff,i}}$ for the different images, this leads to a measurement of D_L^{GW}.

From the expressions in e.g. [93], the significance of having four images can be understood as follows. Let $\boldsymbol{\beta}$ and $\boldsymbol{\theta}_i$ ($i = 1, 2, \ldots, N$) be the angular coordinates on the sky of, respectively, the source displacement from the line of sight to the lens, and the image positions, with N the number of images. To obtain D_L^{GW} from the $D_L^{\mathrm{eff,i}}$, one needs the magnifications

$$\mu_i = [1/\det(\partial\boldsymbol{\beta}/\partial\boldsymbol{\theta})]_{\boldsymbol{\theta}=\boldsymbol{\theta}_i}. \qquad (2)$$

For $N = 4$, $\boldsymbol{\beta}$ and $\boldsymbol{\theta}_i$ (each being two-dimensional) together constitute ten unknowns. As it turns out, ratios of relative time delays only depend on $\boldsymbol{\beta}$ and $\boldsymbol{\theta}_i$, and for four images, there are two independent ones, e.g. $\Delta t_{12}/\Delta t_{13}$ and $\Delta t_{12}/\Delta t_{14}$, whose measurement then provides two constraints on the unknowns. The four image locations are extrema of the Fermat potential $\phi(\boldsymbol{\theta},\boldsymbol{\beta})$, i.e. $\boldsymbol{\nabla}_{\boldsymbol{\theta}}\phi(\boldsymbol{\theta}_i,\boldsymbol{\beta}) = 0$ for $i = 1, \ldots, 4$; assuming that $\phi(\boldsymbol{\theta},\boldsymbol{\beta})$ has been obtained through electromagnetic lens reconstruction, these yield another eight constraints. This is enough information to solve for $\boldsymbol{\beta}$ and $\boldsymbol{\theta}_i$, and hence to obtain the magnifications μ_i through Eq. (2). For $N < 4$, it is still possible to arrive at the μ_i, but one will then need to also rely on the measured relative magnifications μ_i/μ_j to solve for $\boldsymbol{\beta}$ and $\boldsymbol{\theta}_i$. However, relative magnifications usually come with sizeable errors (see e.g. [65]), making $N = 4$ the more interesting case for our purposes.

The details about the EM follow-up and its feasibility are documented in [55,54]. In particular, though Galaxy catalogs are limited in redshift, once a lensed GW event has been identified, dedicated EM follow-ups can be done using e.g. Euclid. Here we consider a scenario where a quadruply lensed GW has already been detected and the host galaxy and lens have been identified and characterized, from which we obtain a measurement of D_L^{GW} as well as a source redshift. By combining the redshift measurement with a cosmology we obtain D_L^{EM}. The two distance measurements, D_L^{GW} and D_L^{EM}, are then used to test the modified propagation theories.

In this work, for definiteness we will assume a flat FLRW universe, in which case one has

$$D_L^{\mathrm{EM}} = \frac{(1+z_s)}{H_0}\int_0^{z_s}\frac{dz'}{E(z')}, \tag{3}$$

where z_s is the redshift of the host galaxy, and $E(z) \equiv \sqrt{\Omega_m(1+z)^3+\Omega_\Lambda}$; here Ω_m and Ω_Λ are the matter and dark energy density parameters, and H_0 is the Hubble constant.

To simulate strongly lensed GWs, we follow [16] and sample BBHs from a POWERLAW+PEAK distribution [94], strongly lensed by a population of Galaxy lenses following the SDSS Galaxy catalog [95]. Our network of detectors consists of the two Advanced LIGO interferometers [2], Advanced Virgo [3], KAGRA [11] and LIGO-India [12], all at design sensitivity. The noise curves of all detectors are implemented using the `bilby.gw.detector` module of the BILBY (version 1.2.1) software package [96]. The events with network signal-to-ratio (SNR) above 8 are considered detected [97]. We then estimate the parameters of the simulated events using GOLUM [65,66], which gives us the effective/measured luminosity distances of each image $D_L^{\mathrm{eff,i}}$ as well as the arrival times. Typically, lens modeling errors and substructure effects will lead to an error budget for the magnification estimates, with ∼10% standard deviation being a reasonable estimate [54,55]. Thus, for each GW measurement, we assume that the magnification posterior derived from the EM band is given by $\mathrm{p}(\mu_i|\vec{d}_{\mathrm{EM}}) = \mathcal{N}(\mu_i|\mu_i^{\mathrm{true}},\sigma_\mu)$, where $\vec{d}_{\mathrm{EM}}$ are the data associated with the EM observations, and $\mathcal{N}(\mu_i|\mu_i^{\mathrm{true}},\sigma_\mu)$ is a normal distribution centered around the true magnification value μ_i^{true} of each image i, with a 10% standard deviation for σ_μ. Doing so allows us to disentangle the intrinsic D_L^{GW} and magnification from $D_L^{\mathrm{eff,i}}$. For the remainder of the discussion, we assume that the intrinsic GW luminosity distance, D_L^{GW}, has been estimated through this procedure.

III. MODIFIED PROPAGATION THEORIES

As explained above, our tests of modified theories of gravity will be based on a comparison between the reconstructed D_L^{GW} and the luminosity distance D_L^{EM} obtained by electromagnetic means.[2] In the specific modified gravity models we consider—large extra dimensions, Ξ-parametrization, and varying Planck mass—there is a nontrivial relationship between these two quantities, which will depend on the parameter(s) related to the deviation from GR and on the cosmological parameters. Let us briefly recall what these relationships look like for our three models.

A. Large extra spatial dimensions

In theories of gravity with large extra dimensions, there is the possibility of some energy of the GWs leaking into them [82,103,104], while EM radiation is confined to the usual three spatial dimensions. This would make the detected signal appear weaker, leading to larger measured values for D_L^{GW} than would otherwise be the case. For definiteness, we will work with the following simple phenomenological ansatz for the relation between D_L^{GW} and D_L^{EM}, based on conservation of integrated flux [60]:

$$D_L^{\mathrm{GW}} = (D_L^{\mathrm{EM}}(z_s,H_0))^{\frac{D-2}{2}}, \tag{4}$$

where D is the number of spacetime dimensions and z_s is the source redshift. We will allow D be a real number, with the GR value $D=4$ as a fiducial value. An illustration of the effect of extra dimensions on a GW waveform is given in the top panel of Fig. 1.

B. Ξ parametrization

Another parametrization was proposed in [62], where the link between D_L^{GW} and D_L^{EM} is expressed as

$$D_L^{\mathrm{GW}} = D_L^{\mathrm{EM}}(z_s,H_0)\left[\Xi_0 + \frac{1-\Xi_0}{(1+z_s)^n}\right]. \tag{5}$$

The free parameters of the model are (Ξ_0, n). This parametrization is phenomenological in nature, but as shown in [63] it can be related to a large class of modified gravity theories, including Horndeski [105] theories, degenerate higher order scalar-tensor theories (DHOST) [106], and theories with nonlocally modified gravity [107–109]. When $z \ll 1$, $D_L^{\mathrm{GW}} \simeq D_L^{\mathrm{EM}}$. Therefore, similar to the extra dimension theories, we expect to observe a departure from GR only at large distances ($z \gtrsim 1$). For GR, $\Xi_0 = 1$ and n is degenerate. In Fig. 1, middle panel, one can see an illustration of the effect of this modified propagation theory on the observed GW signal.

C. Time-varying Planck mass

A time-varying Planck mass is another possible cause for modified GW propagation. Following [61], the relation between D_L^{GW} and D_L^{EM} can be expressed as

$$D_L^{\mathrm{GW}}(z) = D_L^{\mathrm{EM}}(z_s,H_0) \times \exp\left(\frac{c_M}{2\Omega_\Lambda}\ln\frac{1+z_s}{(\Omega_m(1+z_s)^3+\Omega_\Lambda)^{1/3}}\right), \tag{6}$$

[2]Here we will focus exclusively on anomalous propagation affecting the amplitude of GWs, but for models that lead to dispersion, the effect on the GW *phasing* of BBH signals has been used to place very stringent constraints [1,5,98–101]. In addition, the difference between the times of arrival of GW170817 and the associated gamma ray burst has enabled strong constraints on differences between the speed of gravitational waves and the speed of light [102].

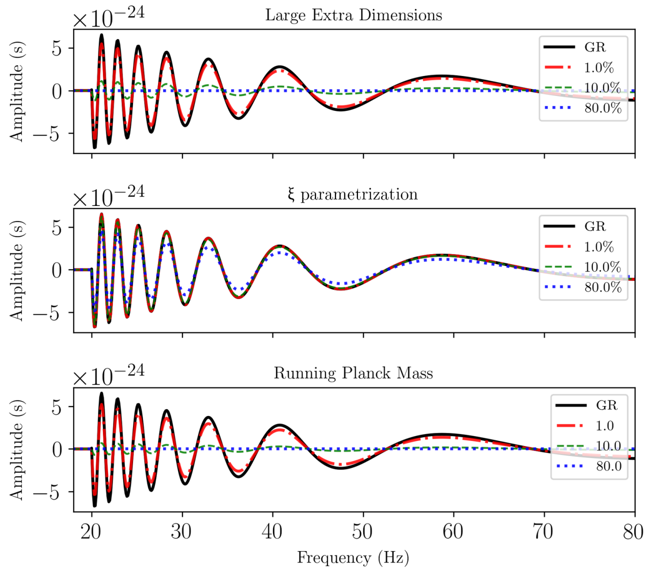

FIG. 1. The effect on the frequency domain GW signal in each of the modified propagation models assuming different amounts of deviations from GR denoted by different colors. In these examples, the GW source is assumed to be at ~5 Gpc, and the rest of the source parameters are similar to those of GW150914 [1]. For the running Planck mass model, the deviation is absolute since one has $c_M = 0$ in GR. For large extra dimensions and Ξ parametrization, we consider percentage deviation in the parameters D and Ξ_0, taking the fiducial values to be $D = 4$ and $\Xi = 1$, respectively. For the Ξ parametrization, we arbitrarily choose $n = 1$ here, though in our subsequent analyses it will be a free parameter.

where c_M is a constant that relates the rate of change of the Planck mass with the fractional dark energy density in the Universe; for details, see Ref. [61] and references therein. For GR, $c_M = 0$. The bottom panel of Fig. 1 illustrates the change in a GW signal in the non-GR case.

IV. METHOD

In this section, we provide a more detailed outline of our method to measure the parameters characterizing the deviation for each case discussed in Sec. III.

We want to measure the deviation parameters given the GW data ($\vec{d}_{\mathrm{GW}}$) and the EM data ($\vec{d}_{\mathrm{EM}}$) associated with a strongly lensed GW with quadruple images whose host galaxy has been determined. Let us denote the deviation parameters in all generality by $\vec{\theta}_{\mathrm{MGR}}$. What we want to obtain is $p(\vec{\theta}_{\mathrm{MGR}}, H_0|\vec{d}_{\mathrm{GW}}, \vec{d}_{\mathrm{EM}})$, the posterior probability distribution of the deviation parameters and the Hubble constant given the observed data. (As explained in the Introduction, other cosmological parameters are given definite values.) Using Bayes' theorem, we can write

$$p(\vec{\theta}_{\mathrm{MGR}}, H_0|\vec{d}_{\mathrm{GW}}, \vec{d}_{\mathrm{EM}}) = \frac{p(\vec{\theta}_{\mathrm{MGR}}, H_0)\, p(\vec{d}_{\mathrm{GW}}, \vec{d}_{\mathrm{EM}}|\vec{\theta}_{\mathrm{MGR}}, H_0)}{Z}, \tag{7}$$

TABLE I. Deviation parameter(s) for each theory and the corresponding prior probability distributions used in our analyses.

Theory	Parameter	Priors
Large extra dimension	D	Uniform (3, 5)
Ξ parametrization	Ξ_0	Log uniform (0.01, 100)
	n	Uniform (0, 10)
Running Planck mass	c_M	Uniform (−150, 150)

where H_0 is the Hubble constant; $p(\vec{\theta}_{\mathrm{MGR}}, H_0)$ the prior probability distribution for $\vec{\theta}_{\mathrm{MGR}}$ and H_0; $p(\vec{d}_{\mathrm{GW}}, \vec{d}_{\mathrm{EM}}|\vec{\theta}_{\mathrm{MGR}}, H_0)$ the likelihood function; and Z the evidence, whose value follows from the requirement that the posterior probability distribution be normalized. The prior distributions for $\vec{\theta}_{\mathrm{MGR}}$ are specified in Table I. We have chosen uninformative priors on each of the $\vec{\theta}_{\mathrm{MGR}}$ parameters in order to not favor any specific value. The ranges of the prior are chosen following the previous studies on constraining the $\vec{\theta}_{\mathrm{MGR}}$ [61,81,83]. As explained in the Introduction, for H_0 we could in principle choose a relatively narrow prior range based on the Planck [77], SHoES [78], or other existing measurements [79]. Instead, we make the more conservative choice of using as a prior the posterior distribution for H_0 obtained from the differences in time of arrival of the GW images, together with lens reconstruction through electromagnetic means. For details we refer to [55,80]; here we confine ourselves to recalling that what is obtained from observations is the so-called time delay distance $D_{\Delta t}$, which is related to H_0 through

$$D_{\Delta t}(z_l, z_s, H_0) = \frac{\int_0^{z_s} dz'/E(z')}{\int_{z_l}^{z_s} dz'/E(z')} D_L^{\mathrm{EM}}(z_s, H_0). \tag{8}$$

Here z_l and z_s are respectively the lens and the source redshift, and $E(z) \equiv \sqrt{\Omega_m(1+z)^3 + \Omega_\Lambda}$. If $D_{\Delta t}$ is measured, we can estimate D_L^{EM} since we assume that z_l and z_s are known from the EM follow-up observations. Using the D_L^{EM} measurement, H_0 can be estimated through Eq. (3). $D_{\Delta t}$ can be measured by performing lens reconstruction; however, owing to the computational complexity and cost, we skip the lens construction step. We assume that the observed value of $D_{\Delta t}$ follows a Gaussian distribution with a 10% standard deviation. To allow for an offset in the observation, we pick the mean of this distribution from another Gaussian distribution with a 10% standard deviation which is centered at the true value. The 10% error assumed in the measurement of $D_{\Delta t}$ is motivated by the results of [55]. We translate the measurement of $D_{\Delta t}$ into the measurement of D_L^{EM} using Eq. (8). Using the value of D_L^{EM} together with Eq. (3), we construct the prior for H_0.

To calculate the likelihood $p(\vec{d}_{\mathrm{GW}}, \vec{d}_{\mathrm{EM}}|\vec{\theta}_{\mathrm{MGR}}, H_0)$, we first express it as

$$p(\vec{d}_{\mathrm{GW}}, \vec{d}_{\mathrm{EM}}|\vec{\theta}_{\mathrm{MGR}}, H_0) = \int d\vec{\theta} dz_s p(\vec{d}_{\mathrm{GW}}|\vec{\theta}) p(\vec{d}_{\mathrm{EM}}|z_s) \times p(\vec{\theta}|z_s, \vec{\theta}_{\mathrm{MGR}}, H_0) p(z_s|\vec{\theta}_{\mathrm{MGR}}, H_0), \tag{9}$$

where $\vec{\theta}$ denotes the GW source parameters, $p(\vec{d}_{\mathrm{GW}}|\vec{\theta})$ and $p(\vec{d}_{\mathrm{EM}}|z_s)$ are the likelihoods of the GW and EM data respectively, and z_s is the source redshift. $p(\vec{\theta}|z_s, \vec{\theta}_{\mathrm{MGR}}, H_0)$ and $p(z_s|\vec{\theta}_{\mathrm{MGR}}, H_0)$ are the priors on the GW source parameters and redshift.

Since we assume that the host galaxy has been localized, the true source redshift z_s is known. Recent studies have shown that the spectroscopic redshift of the source can be measured to a subpercent accuracy [110]. Therefore, we neglect the error on the measurement of z_s so the term $p(\vec{d}_{\mathrm{EM}}|z_s)$ becomes a Dirac delta function centered on z_s, reducing Eq. (9) to

$$p(\vec{d}_{\mathrm{GW}}, \vec{d}_{\mathrm{EM}}|\vec{\theta}_{\mathrm{MGR}}, H_0) = \int d\vec{\theta} p(\vec{d}_{\mathrm{GW}}|\vec{\theta}) p(\vec{\theta}|z_s, \vec{\theta}_{\mathrm{MGR}}, H_0) p(z_s|\vec{\theta}_{\mathrm{MGR}}, H_0). \tag{10}$$

To estimate the GW likelihood $p(\vec{d}_{\mathrm{GW}}|\vec{\theta})$, we perform Bayesian parameter inference using nested sampling [111] for the first image. Subsequently we use GOLUM [65,66] to speed up Bayesian parameter inference for the other images. GOLUM can rapidly analyze lensed images by using the posterior samples of the first image as prior for the subsequent images, as the source parameters for each of the four images are expected to be the same, apart from relative magnifications, rigid phase offsets, and differences in time of arrival.

Once we have the GW likelihood, we perform the integration over the $\vec{\theta}$ for all parameters except the luminosity distance D_L^{GW}, yielding

$$p(\vec{d}_{\mathrm{GW}}, \vec{d}_{\mathrm{EM}}|\vec{\theta}_{\mathrm{MGR}}, H_0) = \int dD_L^{\mathrm{GW}} p(\vec{d}_{\mathrm{GW}}|D_L^{\mathrm{GW}}) p(D_L^{\mathrm{GW}}|z_s, \vec{\theta}_{\mathrm{MGR}}, H_0) \times p(z_s|\vec{\theta}_{\mathrm{MGR}}, H_0). \tag{11}$$

The prior $p(D_L^{\mathrm{GW}}|z_s, \vec{\theta}_{\mathrm{MGR}}, H_0)$ reduces to a Dirac delta function as we exactly know D_L^{GW} given the values of z_s, $\vec{\theta}_{\mathrm{MGR}}$, H_0 and the modified gravity model [Eqs. (4), (5) and (6)]. Therefore, integrating with respect to D_L^{GW} leads to

$$p(\vec{d}_{\mathrm{GW}}, \vec{d}_{\mathrm{EM}}|\vec{\theta}_{\mathrm{MGR}}, H_0) = p(\vec{d}_{\mathrm{GW}}|D_L^{\mathrm{GW}}) p(z_s|\vec{\theta}_{\mathrm{MGR}}, H_0). \tag{12}$$

Substituting Eq. (12) into Eq. (7), we can obtain the posterior distributions for $\vec{\theta}_{\mathrm{MGR}}$ and H_0. The above derivation is performed for one of the images of the quadruplet. To combine the information from multiple images and obtain the joint posterior on $\vec{\theta}_{\mathrm{MGR}}$, we need to express the distance likelihood $p(\vec{d}_{\mathrm{GW}}|D_L^{\mathrm{GW}})$ in Eq. (12) as a joint likelihood:

$$p(\vec{d}_{\mathrm{GW}}|D_L^{\mathrm{GW}}) = \prod_{i=0}^{3} p(\vec{d}_{\mathrm{GW},i}|D_L^{\mathrm{GW}}), \tag{13}$$

where $\vec{d}_{\mathrm{GW},i}$ refers to the GW data from image i.

In what follows, we assume binary black hole coalescences with component mass distributions drawn from the POWERLAW+PEAK in [94]. Our GW waveform model is IMRPHENOMXPHM [112], with black hole spin magnitudes distributed uniformly between 0 and 1, and spin directions uniformly on the sphere. The distribution of the redshifts of the BBH and the galaxy lenses (modeled as singular power law isothermal ellipsoids with external shear) is obtained from [16]. The fiducial values of $\vec{\theta}_{\mathrm{MGR}}$ are equal to their GR values. The fiducial value of the Hubble constant is $H_0 = 67.4\ \mathrm{km\,s^{-1}\,Mpc^{-1}}$, and $\Omega_m = 0.315$. The lensed GWs were analyzed using GOLUM [65,66] and DYNESTY [113] to produce the D_L^{GW} posteriors along with other source parameters. Our detector network consists of two LIGO [2], the Virgo [3], the KAGRA [11], and the LIGO-India [12] detectors where the detection threshold on the network SNR is 8. Results obtained using lensed events will be compared with what can be obtained from the GW observation of the BNS merger GW170817 together with its host galaxy identification [114]. For GW170817, we use the D_L^{GW} posterior sample from the corresponding data release [115]. For this event we cannot construct the prior on H_0 for GW170817 using the method which we used for lensed events; therefore we use Planck 2018 [76] results when analyzing it.

V. RESULTS

Before diving into the full parameter estimation results, we first look into how the relative difference $\Delta = |D_L^{\mathrm{GW}} - D_L^{\mathrm{EM}}|/D_L^{\mathrm{EM}}$ varies as a function of z_s and $\vec{\theta}_{\mathrm{MGR}}$, to help us understand how large the imprint of various deviations will be. Values for Δ are indicated by the color coding in Fig. 2. Here D_L^{EM} is calculated for a range of values for redshift (horizontal axis), and D_L^{GW} is computed using Eqs. (4)–(6) for a variety of (relative) deviation parameters (vertical axis). If Δ is small (dark regions), there may only be a negligible imprint in the departure from GR

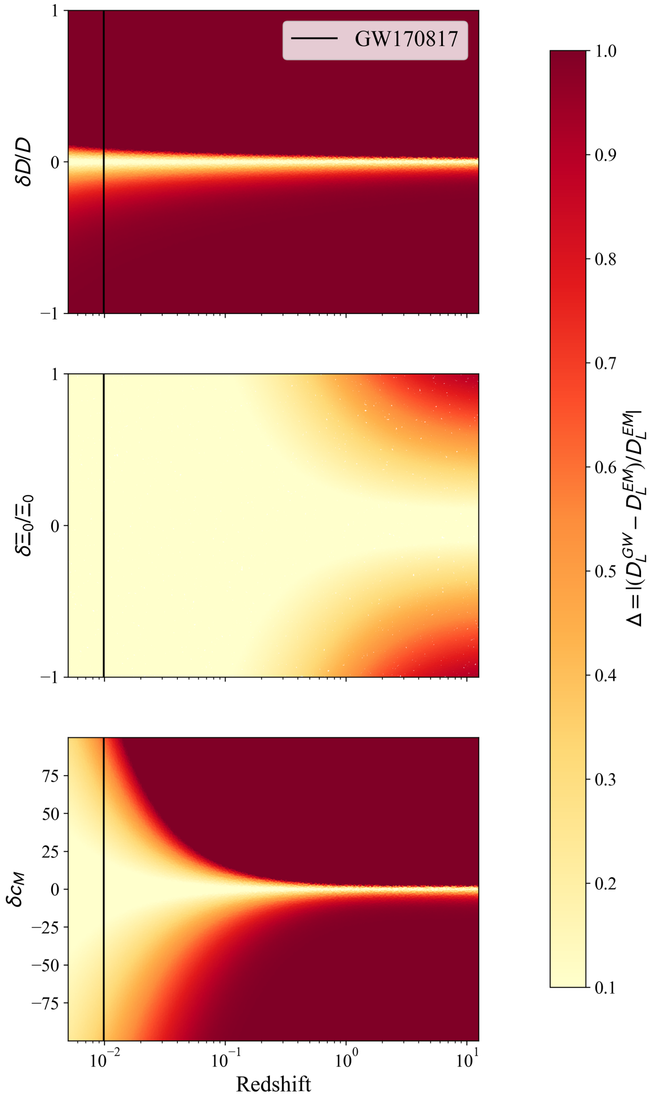

FIG. 2. The fractional difference $\Delta \equiv |(D_L^{\mathrm{GW}} - D_L^{\mathrm{EM}})/D_L^{\mathrm{EM}}|$ (color) between D_L^{GW} and D_L^{EM} as a function of source redshift (horizontal axis) and deviation parameter (vertical axis). The $\delta D/D$ (top panel) and $\delta\Xi_0/\Xi_0$ (middle) refer to changes in respectively D and Ξ_0 relative to their fiducial values $D = 4$ and $\Xi_0 = 1$ (with $n = 1$ for the latter case), whereas for c_M (bottom panel) we use the value of the parameter itself. In the light (dark) regions the impact of the deviation parameter on the relation between D_L^{GW} and D_L^{EM} is larger (smaller). At the redshift of GW170817 (green vertical line), for the Ξ parametrization and varying Planck mass, Δ is smaller than at high redshifts, already suggesting that strong lensing measurements, which access the high-redshift regime, are likely to lead to better constraints on these deviation parameters. On the other hand, the effect of extra dimensions is less sensitive to redshift, and measurements of D are not expected to improve as much as for the other two cases.

even if the deviation parameter differs significantly from its GR value. In the light regions, we have a better chance of observing a deviation from GR if it is present.

The green vertical line shows the measured redshift of the host galaxy of GW170817 ($z \simeq 0.009783$ [116,117]). For the extra dimensions model, the line is mainly in the light region, making the imprint of the deviation relatively large even for relatively small departures from the fiducial value of $D = 4$. However, for the given ranges of the Ξ_0 and c_M parameters, GW170817 stays mostly in the dark regions, making it more difficult to find the corresponding deviations from GR. In the latter two cases, higher redshifts than that of GW170817 are needed to have significantly better bounds on Ξ_0 and c_M, and this is what GW lensing will provide.

In Fig. 3, we present the results obtained from a detailed simulation, as explained in the previous section. We consider a total of 55 GW events for the analysis.[3] Each dot in Fig. 3 corresponds to a simulated strongly lensed GW event with quadruple images, at a given source redshift (horizontal axis), analyzed as described in Sec. IV. The true values of deviation parameters are set equal to their GR values. The vertical axis indicates the 90% confidence intervals for relative deviations in D (top) and Ξ_0 (center), and for the absolute deviation in c_M (bottom), as the latter parameter is zero in GR. Since in the Ξ parametrization, the parameter n is unconstrained when Ξ_0 equals its fiducial value of 1, we do not show results for it here, though it was treated as a free parameter in our measurements. Finally, the color coding shows the combined SNR from the four images, i.e. the quadrature sum of the SNRs of the individual images. Also included are results from GW170817.

The results are in qualitative agreement with Fig. 2. In particular, for Ξ_0 and c_M the advantage of being able to access higher redshifts is clearly in evidence, with bounds improving over those of GW170817 by factors of up to $\mathcal{O}(10)$ and $\mathcal{O}(100)$, respectively. By contrast, the bounds on D improve by up to a factor of ~ 5. The differences in improvement can be explained by the qualitative predictions of Fig. 2 where Δ follows a steep gradient for Ξ_0 (center) and c_M (bottom) but a shallow one for D (top).

We note that for the strongly lensed events in our catalog, the combined SNR from the four images tends to be higher than that of GW170817, which can also improve the measurement accuracy on D_L^{GW} and $\vec{\theta}_{\mathrm{MGR}}$. Indeed, the measurement of the parameters is done using combined information from the different images, increasing the effective SNR used to infer the parameters values. However, in Fig. 3 we observe that lensed events with SNR similar to GW170817 (which was $\simeq 32.4$ [84]) can measure the $\vec{\theta}_{\mathrm{MGR}}$ more accurately compared to the latter as the lensed events are placed at high redshifts. Therefore, an increment in the distance made accessible by strong lensing

[3]Note that we do not expect to see this many quadruply lensed events until the third-generation detector era; nor do we combine information from multiple simulated lensed events. Our aim here is to explore the diversity of scenarios one might encounter for single quadruply lensed GW.

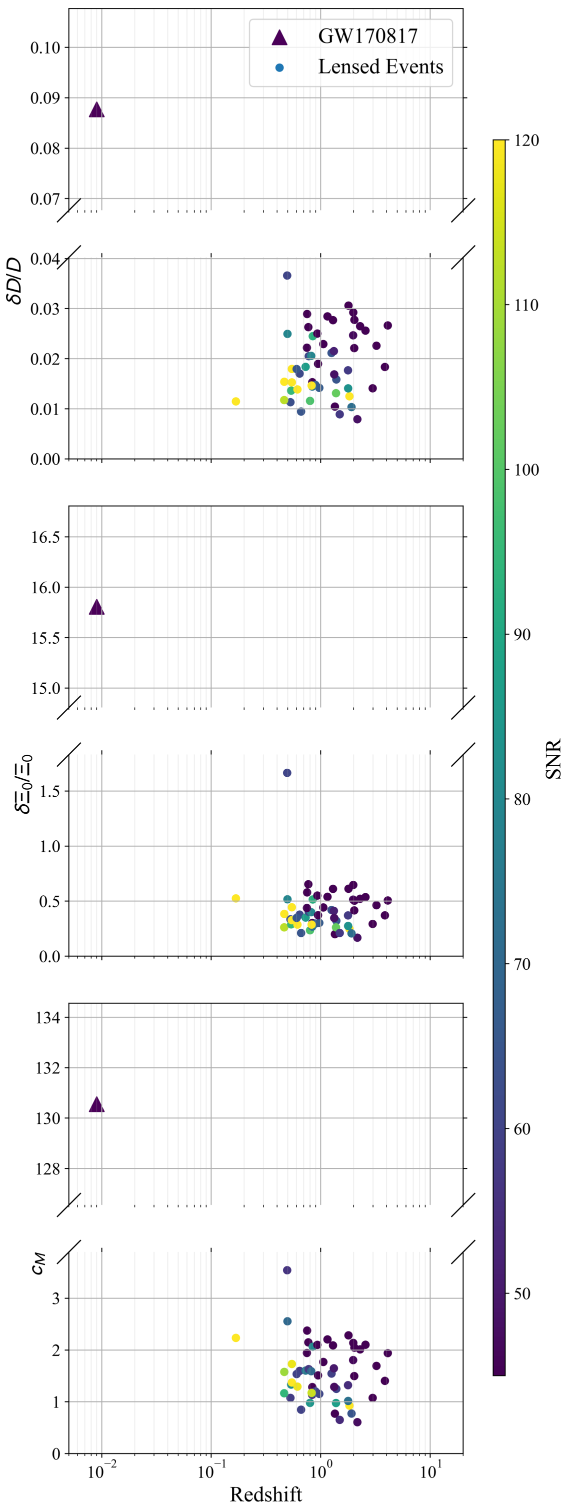

FIG. 3. 90% confidence intervals for measurements of $\delta D/D$, $\delta\Xi_0/\Xi_0$ (defined as in Fig. 2) and c_M. The dots refer to results from quadruply lensed events, whose source redshifts can be read off from the horizontal axis; in each case the colors indicate the combined SNRs from the four images. The triangle indicates bounds from GW170817. Even lensed events with combined SNR similar to that of GW170817 (which was $\simeq$32.4) yield considerably better constraints on deviation parameters, again underscoring the benefit of being able to access the high-redshift regime.

is indeed the dominating factor in the improvement of measurement accuracies.

For the Ξ parametrization, bounds we obtain from our simulated lensed events are consistent with the results of Finke *et al.* [64]. Let us also make a comparison with existing bounds from actual measurements. We have already mentioned the improvements of bounds from lensing with respect to measurements done with GW170817. In Mastrogiovanni *et al.* [81], bounds were obtained for the three models considered here, by combining information from GW170817 and its EM counterpart with information from the BBH signal GW190521, in the latter case assuming that a particular EM flare observed by the Zwicky Transient Factory (ZTF) [118] was associated with the BBH merger. Since GW190521 originated at a redshift of $\simeq$0.8 [119], adding this event brings the bounds on deviation parameters closer to what we find for lensed events; for example, they report $\delta\Xi_0/\Xi_0 \lesssim 3$–10 depending on assumptions made, to be compared with the bounds in Fig. 3.[4] When specific alternative theories of gravity are assumed, studies based on the Cosmic Microwave Background and large structure formation can lead to bounds on c_M that are similar to the ones for lensed events; see e.g. [121] and the discussion in [61]. Finally, methods have developed that exploit the observed population properties of binary black hole coalescences using gravitational wave data only, in terms of e.g. redshift and mass distributions [86–88]. Depending on the assumptions made, these can be competitive with bounds on anomalous GW propagation that we project for lensed GW events with host galaxy identification.

Finally, though we did not perform simulations for GR violating lensed GW events, it seems reasonable to assume that the bounds we find on relevant parameters will be indicative of how large a GR violation would need to be in each of the three models in order to be detectable.

VI. CONCLUSIONS AND FUTURE DIRECTIONS

Strong lensing of GWs could be detected in the near future, and there are various applications to be developed thanks to the additional information it can provide. Here we have focused on the fact that, under favorable circumstances, a quadruply lensed GW event together with EM observations can enable the identification of the host galaxy of a BBH event. In turn, this opens up the possibility of constraining alternative theories of gravity that predict anomalous GW propagation, by comparing the luminosity distance D_L^{EM} that is obtained electromagnetically with the luminosity distance D_L^{GW} obtained from the GW if the amplitude of the latter is assumed to be proportional to $1/D_L^{\mathrm{GW}}$. Three heuristic relationships between D_L^{GW} and

[4]However, it should be noted that the association of GW190521 with the EM flare of [118] is by no means conclusive; see e.g. [120].

D_L^{EM} were considered, motivated by large extra spatial dimensions, a variable Planck mass, and the so-called Ξ parametrization which captures anomalous propagation effects in a variety of alternative theories.

To study what kinds of constraints can be put on these non-GR models using lensed GW events, we set up an extensive simulation, making use of realistic lens and BBH source populations to arrive at plausible distributions for the properties of quadruply lensed events. We performed Bayesian inference on each of the simulated GW events to obtain posterior density distributions for their parameters. Due to the associated computational complexity and cost, we did not directly perform lens reconstruction, but instead assumed Gaussian probability distributions for image magnification measurements used in the reconstruction of D_L^{GW}, as well as for reconstructed electromagnetic luminosity distances, with widths informed by current astrophysical expectations [54,55]. The latter aspect is something we aim to treat in more depth in a future study. Similarly, the relation between D_L^{GW} and D_L^{EM} involves cosmological parameters; in this work we only let H_0 be a free parameter, but the effect of uncertainties in the other parameters is also worth investigating. On the other hand, in this study we used as a prior on H_0 the posterior density distribution obtained from time delay measurements and lens reconstruction, which is typically considerably wider than the ranges for H_0 obtained from either Planck or SHoES [55]. Because of the degeneracy between H_0 and the deviation parameters, bounds on the latter are to a large extent set by the prior range of H_0 [61], which pushes our constraints on alternative theories toward the conservative side.[5]

The indicator of deviation from GR on the GW signal in all three cases—larger extra dimensions, Ξ parametrization, and time-varying Planck mass—is the change in the amplitude of the signal (Fig. 1). The magnitude of change varies from one case to another, raising the possibility that a strong deviation from GR in one model (Ξ parametrization, for example) is detected as a weak deviation in other models (larger extra dimensions and time-varying Planck mass). However, in our work, we have not considered the possibility of model misclassification; this we leave for future work.

Comparing with results from GW170817 and its EM counterpart (for which we did use the much more narrow H_0 prior from Planck 2018 [76]), we clearly see the effect of strongy lensed GWs from BBH typically originating from much higher redshifts. The latter improves the measurability of anomalous propagation, since it increases with distance. In the case of extra dimensions, modest gains by up to a factor of ~ 5 are seen, but for the Ξ parametrization this becomes $\mathcal{O}(10)$, and for c_M as much as $\mathcal{O}(100)$.

Previous GW-based measurements on anomalous propagation models [61,62,81–83] have utilized GW170817 with its EM counterpart (and GW190521 under the assumption that an EM flare seen by ZTF was an EM counterpart to this BBH event). Until the advent of third-generation GW observatories such as the Einstein Telescope [122–124] and Cosmic Explorer [125,126], GW signals from binary neutron star inspirals will only be seen to redshifts $z \ll 1$ [127], and the definitive identification of transient EM counterparts to stellar mass BBH events may remain elusive. Other methods based on the population properties of binary black holes inferred from GW data alone have been shown to considerably improve over bounds from multimessenger observations of GW170817 [86–88]. What we have demonstrated here is that a single fortuitous discovery of a quadruply lensed GW event in conjunction with EM observations of lensed galaxies may give access to the high-redshift regime, again enabling significantly stronger constraints on models of anomalous GW propagation.

ACKNOWLEDGMENTS

The authors would like to thank Simone Mastrogiovannni, Jason Poon, and Ewoud Wempe for useful discussions. H. N., J. J., K. H., and C. V. D. B. are supported by the research program of the Netherlands Organisation for Scientific Research (NWO). L. H. is supported by the Swiss National Science Foundation Grant No. 199307, as well as the European Union's Horizon 2020 research and innovation program under the Marie Skłodowska-Curie Grant Agreement No. 945298-ParisRegionFP. She is a Fellow of Paris Region Fellowship Programme supported by the Paris Region, and acknowledges the support of the COST Action CA18108. The authors are grateful for computational resources provided by the LIGO Laboratory and supported by the National Science Foundation Grants No. PHY-0757058 and No. PHY-0823459. This research has made use of data, software and/or web tools obtained from the Gravitational Wave Open Science Center [128], a service of LIGO Laboratory, the LIGO Scientific Collaboration and the Virgo Collaboration. LIGO is funded by the U.S. National Science Foundation. Virgo is funded by the French Centre National de Recherche Scientifique (CNRS), the Italian Istituto Nazionale della Fisica Nucleare (INFN) and the Dutch Nikhef, with contributions by Polish and Hungarian institutes.

[5]When analyzing the lensed events with a prior from Planck 2018 [76] we obtain bounds that are a factor of ~ 2 tighter.

[1] B. P. Abbott et al. (LIGO Scientific and Virgo Collaborations), Phys. Rev. Lett. **116**, 061102 (2016).
[2] J. Aasi et al. (LIGO Scientific Collaboration), Classical Quantum Gravity **32**, 074001 (2015).
[3] F. Acernese et al. (Virgo Collaboration), Classical Quantum Gravity **32**, 024001 (2015).
[4] R. Abbott et al. (LIGO Scientific, Virgo, and KAGRA Collaborations), Phys. Rev. X **13**, 041039 (2023).
[5] R. Abbott et al. (LIGO Scientific, Virgo, and KAGRA Collaborations), arXiv:2112.06861.
[6] R. Abbott et al. (LIGO Scientific, Virgo, and KAGRA Collaborations), Astrophys. J. **949**, 76 (2023).
[7] R. Abbott et al. (LIGO Scientific, Virgo, and KAGRA Collaborations), arXiv:2111.03634.
[8] K. Somiya (KAGRA Collaboration), Classical Quantum Gravity **29**, 124007 (2012).
[9] Y. Aso, Y. Michimura, K. Somiya, M. Ando, O. Miyakawa, T. Sekiguchi, D. Tatsumi, and H. Yamamoto (KAGRA Collaboration), Phys. Rev. D **88**, 043007 (2013).
[10] T. Akutsu et al. (KAGRA Collaboration), Nat. Astron. **3**, 35 (2019).
[11] T. Akutsu et al. (KAGRA Collaboration), Prog. Theor. Exp. Phys. **2021**, 05A101 (2021).
[12] C. S. Unnikrishnan, Int. J. Mod. Phys. D **22**, 1341010 (2013).
[13] R. Takahashi and T. Nakamura, Astrophys. J. **595**, 1039 (2003).
[14] R. Takahashi, Astrophys. J. **644**, 80 (2005).
[15] M. Oguri and R. Takahashi, arXiv:2204.00814.
[16] A. R. A. C. Wierda, E. Wempe, O. A. Hannuksela, L. e. V. E. Koopmans, and C. Van Den Broeck, Astrophys. J. **921**, 154 (2021).
[17] K. K. Y. Ng, K. W. K. Wong, T. Broadhurst, and T. G. F. Li, Phys. Rev. D **97**, 023012 (2018).
[18] F. Xu, J. M. Ezquiaga, and D. E. Holz, Astrophys. J. **929**, 9 (2022).
[19] M. Oguri, Mon. Not. R. Astron. Soc. **480**, 3842 (2018).
[20] S. Mukherjee, T. Broadhurst, J. M. Diego, J. Silk, and G. F. Smoot, Mon. Not. R. Astron. Soc. **506**, 3751 (2021).
[21] G. P. Smith, A. Robertson, G. Mahler, M. Nicholl, D. Ryczanowski, M. Bianconi, K. Sharon, R. Massey, J. Richard, and M. Jauzac, arXiv:2204.12977.
[22] S.-S. Li, S. Mao, Y. Zhao, and Y. Lu, Mon. Not. R. Astron. Soc. **476**, 2220 (2018).
[23] T. E. Collett et al., Astrophys. J. **843**, 148 (2017).
[24] L. Dai and T. Venumadhav, arXiv:1702.04724.
[25] J. M. Ezquiaga, D. E. Holz, W. Hu, M. Lagos, and R. M. Wald, Phys. Rev. D **103**, 064047 (2021).
[26] K.-H. Lai, O. A. Hannuksela, A. Herrera-Martín, J. M. Diego, T. Broadhurst, and T. G. F. Li, Phys. Rev. D **98**, 083005 (2018).
[27] P. Christian, S. Vitale, and A. Loeb, Phys. Rev. D **98**, 103022 (2018).
[28] A. J. Singh, I. S. C. Li, O. A. Hannuksela, T. G. F. Li, and K. Kim, Am. J. Undergrad. Res. **16**, 5 (2018).
[29] L. Dai, S.-S. Li, B. Zackay, S. Mao, and Y. Lu, Phys. Rev. D **98**, 104029 (2018).
[30] K. Kim, J. Lee, R. S. H. Yuen, O. A. Hannuksela, and T. G. F. Li, Astrophys. J. **915**, 119 (2020).
[31] M. H. Y. Cheung, J. Gais, O. A. Hannuksela, and T. G. F. Li, Mon. Not. R. Astron. Soc. **503**, 3326 (2020).
[32] S. M. C. Yeung, M. H. Y. Cheung, J. A. J. Gais, O. A. Hannuksela, and T. G. F. Li, arXiv:2112.07635.
[33] O. Bulashenko and H. Ubach, arXiv:2112.10773.
[34] E. Seo, O. A. Hannuksela, and T. G. F. Li, arXiv:2110.03308.
[35] G. Tambalo, M. Zumalacárregui, L. Dai, and M. H.-Y. Cheung, Phys. Rev. D **108**, 043527 (2023).
[36] M. Wright and M. Hendry, Astrophys. J. **935**, 68 (2022).
[37] S. Deguchi and W. D. Watson, Astrophys. J. **307**, 30 (1986).
[38] T. Baker and M. Trodden, Phys. Rev. D **95**, 063512 (2017).
[39] T. E. Collett and D. Bacon, Phys. Rev. Lett. **118**, 091101 (2016).
[40] K. Liao, X. L. Fan, X. Ding, M. Biesiada, and Z. H. Zhu, Nat. Commun. **8**, 1 (2017).
[41] X. L. Fan, K. Liao, M. Biesiada, A. Piórkowska-Kurpas, and Z. H. Zhu, Phys. Rev. Lett. **118**, 091102 (2017).
[42] K. Liao, X. Ding, M. Biesiada, X.-L. Fan, and Z.-H. Zhu, Astrophys. J. **867**, 69 (2018).
[43] J. M. Diego, Phys. Rev. D **101**, 123512 (2019).
[44] X.-L. Fan, K. Liao, M. Biesiada, A. Piorkowska-Kurpas, and Z.-H. Zhu, Phys. Rev. Lett. **118**, 091102 (2017).
[45] K.-H. Lai, O. A. Hannuksela, A. Herrera-Martín, J. M. Diego, T. Broadhurst, and T. G. F. Li, Phys. Rev. D **98**, 083005 (2018).
[46] P. Cremonese, J. M. Ezquiaga, and V. Salzano, Phys. Rev. D **104**, 023503 (2021).
[47] S. Mukherjee, B. D. Wandelt, and J. Silk, Phys. Rev. D **101**, 103509 (2019).
[48] S. Mukherjee, B. D. Wandelt, and J. Silk, Mon. Not. R. Astron. Soc. **494**, 1956 (2019).
[49] M. Oguri and R. Takahashi, Astrophys. J. **901**, 58 (2020).
[50] S. Goyal, K. Haris, A. K. Mehta, and P. Ajith, Phys. Rev. D **103**, 024038 (2021).
[51] S. Birrer, M. Millon, D. Sluse, A. J. Shajib, F. Courbin, L. V. E. Koopmans, S. H. Suyu, and T. Treu, arXiv:2210.10833.
[52] S. Basak, A. Ganguly, K. Haris, S. Kapadia, A. K. Mehta, and P. Ajith, Astrophys. J. Lett. **926**, L28 (2022).
[53] J. M. Ezquiaga, W. Hu, M. Lagos, M.-X. Lin, and F. Xu, J. Cosmol. Astropart. Phys. 08 (2022) 016.
[54] E. Wempe, L. V. E. Koopmans, A. R. A. C. Wierda, O. A. Hannuksela, and C. v. d. Broeck, arXiv:2204.08732.
[55] O. A. Hannuksela, T. E. Collett, M. Çalişkan, and T. G. F. Li, Mon. Not. R. Astron. Soc. **498**, 3395 (2020).
[56] G. Tambalo, M. Zumalacárregui, L. Dai, and M. H.-Y. Cheung, Phys. Rev. D **108**, 103529 (2023).
[57] S. Vegetti et al., arXiv:2306.11781.
[58] J. M. Ezquiaga and M. Zumalacárregui, Phys. Rev. D **102**, 124048 (2020).
[59] S. Goyal, A. Vijaykumar, J. M. Ezquiaga, and M. Zumalacarregui, Phys. Rev. D **108**, 024052 (2023).
[60] C. Deffayet and K. Menou, Astrophys. J. Lett. **668**, L143 (2007).
[61] M. Lagos, M. Fishbach, P. Landry, and D. E. Holz, Phys. Rev. D **99**, 083504 (2019).
[62] E. Belgacem, Y. Dirian, S. Foffa, and M. Maggiore, Phys. Rev. D **98**, 023510 (2018).
[63] E. Belgacem et al. (LISA Cosmology Working Group), J. Cosmol. Astropart. Phys. 07 (2019) 024.

[64] A. Finke, S. Foffa, F. Iacovelli, M. Maggiore, and M. Mancarella, Phys. Rev. D **104**, 084057 (2021).
[65] J. Janquart, O. A. Hannuksela, H. K., and C. Van Den Broeck, Mon. Not. R. Astron. Soc. **506**, 5430 (2021).
[66] J. Janquart, K. Haris, O. A. Hannuksela, and C. Van Den Broeck, Mon. Not. R. Astron. Soc. **526**, 3088 (2023).
[67] R. K. L. Lo and I. Magaña Hernandez, Phys. Rev. D **107**, 123015 (2023).
[68] O. A. Hannuksela, T. E. Collett, M. Çalişkan, and T. G. F. Li, Mon. Not. R. Astron. Soc. **498**, 3395 (2020).
[69] N. Seto, Phys. Rev. D **69**, 022002 (2004).
[70] H.-Y. Chen, M. Fishbach, and D. E. Holz, Nature (London) **562**, 545 (2018).
[71] M. Fishbach *et al.* (LIGO Scientific and Virgo Collaborations), Astrophys. J. Lett. **871**, L13 (2019).
[72] R. Gray *et al.*, Phys. Rev. D **101**, 122001 (2020).
[73] B. P. Abbott *et al.* (LIGO Scientific and Virgo Collaborations), Astrophys. J. **909**, 218 (2021).
[74] M. Soares-Santos *et al.* (DES, LIGO Scientific, and Virgo Collaborations), Astrophys. J. Lett. **876**, L7 (2019).
[75] D. W. Hogg, arXiv:astro-ph/9905116.
[76] N. Aghanim *et al.* (Planck Collaboration), Astron. Astrophys. **641**, A6 (2020); **652**, C4(E) (2021).
[77] Planck Collaboration, arXiv:astro-ph/0604069.
[78] A. G. Riess *et al.*, Astrophys. J. Lett. **934**, L7 (2022).
[79] K. C. Wong *et al.*, Mon. Not. R. Astron. Soc. **498**, 1420 (2020).
[80] E. Wempe, L. V. E. Koopmans, A. R. A. C. Wierda, O. A. Hannuksela, and C. v. d. Broeck, arXiv:2204.08732.
[81] S. Mastrogiovanni, L. Haegel, C. Karathanasis, I. M. n. Hernandez, and D. A. Steer, J. Cosmol. Astropart. Phys. 02 (2021) 043.
[82] B. P. Abbott *et al.* (LIGO Scientific and Virgo Collaborations), Phys. Rev. Lett. **123**, 011102 (2019).
[83] K. Pardo, M. Fishbach, D. E. Holz, and D. N. Spergel, J. Cosmol. Astropart. Phys. 07 (2018) 048.
[84] B. P. Abbott *et al.* (LIGO Scientific and Virgo Collaborations), Phys. Rev. Lett. **119**, 161101 (2017).
[85] B. P. Abbott *et al.* (LIGO Scientific, Virgo, Fermi GBM, INTEGRAL, IceCube, AstroSat Cadmium Zinc Telluride Imager Team, IPN, Insight-Hxmt, ANTARES, Swift, AGILE Team, 1M2H Team, Dark Energy Camera GW-EM, DES, DLT40, GRAWITA, Fermi-LAT, ATCA, ASKAP, Las Cumbres Observatory Group, OzGrav, DWF (Deeper Wider Faster Program), AST3, CAASTRO, VINROUGE, MASTER, J-GEM, GROWTH, JAGWAR, CaltechNRAO, TTU-NRAO, NuSTAR, Pan-STARRS, MAXI Team, TZAC Consortium, KU, Nordic Optical Telescope, ePESSTO, GROND, Texas Tech University, SALT Group, TOROS, BOOTES, MWA, CALET, IKI-GW Follow-up, H.E.S.S., LOFAR, LWA, HAWC, Pierre Auger, ALMA, Euro VLBI Team, Pi of Sky, Chandra Team at McGill University, DFN, ATLAS Telescopes, High Time Resolution Universe Survey, RIMAS, RATIR, SKA South Africa/MeerKAT Collaborations), Astrophys. J. Lett. **848**, L12 (2017).
[86] J. M. Ezquiaga, Phys. Lett. B **822**, 136665 (2021).
[87] K. Leyde, S. Mastrogiovanni, D. A. Steer, E. Chassande-Mottin, and C. Karathanasis, J. Cosmol. Astropart. Phys. 09 (2022) 012.
[88] I. Magana Hernandez, Phys. Rev. D **107**, 084033 (2023).
[89] K. Haris, A. K. Mehta, S. Kumar, T. Venumadhav, and P. Ajith, arXiv:1807.07062.
[90] X. Liu, I. M. Hernandez, and J. Creighton, Astrophys. J. **908**, 97 (2020).
[91] S. Goyal, H. D., S. J. Kapadia, and P. Ajith, Phys. Rev. D **104**, 124057 (2021).
[92] S. Birrer and A. Amara, Phys. Dark Universe, **22**, 189 (2018).
[93] G. Pagano, O. A. Hannuksela, and T. G. F. Li, Astron. Astrophys. **643**, A167 (2020).
[94] R. Abbott *et al.* (KAGRA, Virgo, and LIGO Scientific Collaborations), Phys. Rev. X **13**, 011048 (2023).
[95] M. R. Blanton *et al.* (SDSS Collaboration), Astron. J. **154**, 28 (2017).
[96] G. Ashton *et al.*, Astrophys. J. Suppl. Ser. **241**, 27 (2018).
[97] B. P. Abbott *et al.* (KAGRA, LIGO Scientific, and Virgo Collaborations), Living Rev. Relativity **21**, 3 (2018).
[98] B. P. Abbott *et al.* (LIGO Scientific and Virgo Collaborations), Phys. Rev. Lett. **116**, 221101 (2016); **121**, 129902 (E) (2018).
[99] B. P. Abbott *et al.* (LIGO Scientific and Virgo Collaborations), Phys. Rev. Lett. **118**, 221101 (2017); **121**, 129901 (E) (2018).
[100] B. P. Abbott *et al.* (LIGO Scientific and Virgo Collaborations), Phys. Rev. D **100**, 104036 (2019).
[101] R. Abbott *et al.* (LIGO Scientific and Virgo Collaborations), Phys. Rev. D **103**, 122002 (2021).
[102] B. P. Abbott *et al.* (LIGO Scientific, Virgo, Fermi-GBM, and INTEGRAL Collaborations), Astrophys. J. Lett. **848**, L13 (2017).
[103] G. R. Dvali, G. Gabadadze, and M. Porrati, Phys. Lett. B **485**, 208 (2000).
[104] G. Calcagni, S. Kuroyanagi, S. Marsat, M. Sakellariadou, N. Tamanini, and G. Tasinato, Phys. Lett. B **798**, 135000 (2019).
[105] G. W. Horndeski, Int. J. Theor. Phys. **10**, 363 (1974).
[106] D. Langlois, Int. J. Mod. Phys. D **28**, 1942006 (2019).
[107] M. Maggiore, Phys. Rev. D **89**, 043008 (2014).
[108] M. Maggiore and M. Mancarella, Phys. Rev. D **90**, 023005 (2014).
[109] E. Belgacem, Y. Dirian, S. Foffa, and M. Maggiore, J. Cosmol. Astropart. Phys. 03 (2018) 002.
[110] X. Zhou, Y. Gong, X.-M. Meng, X. Zhang, Y. Cao, X. Chen, V. Amaro, Z. Fan, and L. Fu, Astrophys. J. **909**, 53 (2021).
[111] J. Skilling, Bayesian Anal. **1**, 833 (2006).
[112] G. Pratten *et al.*, Phys. Rev. D **103**, 104056 (2021).
[113] J. S. Speagle, Mon. Not. R. Astron. Soc. **493**, 3132 (2019).
[114] B. P. Abbott *et al.* (LIGO Scientific, Virgo, 1M2H, Dark Energy Camera GW-E, DES, DLT40, Las Cumbres Observatory, VINROUGE, MASTER Collaborations), Nature (London) **551**, 85 (2017).
[115] The LIGO Scientific and the Virgo Collaborations, Parameter estimation sample release for GWTC-1 (2020), 10.7935/KSX7-QQ51.
[116] A. J. Levan *et al.*, Astrophys. J. Lett. **848**, L28 (2017).
[117] J. Hjorth, A. J. Levan, N. R. Tanvir, J. D. Lyman, R. Wojtak, S. L. Schrøder, I. Mandel, C. Gall, and S. H. Bruun, Astrophys. J. Lett. **848**, L31 (2017).

[118] M. J. Graham *et al.*, Phys. Rev. Lett. **124**, 251102 (2020).
[119] R. Abbott *et al.* (LIGO Scientific and Virgo Collaborations), Phys. Rev. Lett. **125**, 101102 (2020).
[120] G. Ashton, K. Ackley, I. M. n. Hernandez, and B. Piotrzkowski, Classical Quantum Gravity **38**, 235004 (2021).
[121] J. Noller and A. Nicola, Phys. Rev. D **99**, 103502 (2019).
[122] S. Hild *et al.*, Classical Quantum Gravity **28**, 094013 (2011).
[123] M. Punturo *et al.*, Classical Quantum Gravity **27**, 194002 (2010).
[124] M. Maggiore, C. v. d. Broeck, N. Bartolo, E. Belgacem, D. Bertacca, M. A. Bizouard, M. Branchesi, S. Clesse, S. Foffa, J. García-Bellido, S. Grimm, J. Harms, T. Hinderer, S. Matarrese, C. Palomba, M. Peloso, A. Ricciardone, and M. Sakellariadou, J. Cosmol. Astropart. Phys. 03 (2020) 050.
[125] B. P. Abbott *et al.*, Classical Quantum Gravity **34**, 044001 (2017).
[126] D. Reitze *et al.*, Bull. Am. Astron. Soc. **51**, 035 (2019).
[127] B. P. Abbott *et al.*, Living Rev. Relativity **21**, 3 (2018).
[128] https://www.gw-openscience.org.